ACS APPLIED MATERIALS & INTERFACES

Research Article

www.acsami.org

Influence of Protein Corona on the Transport of Molecules into Cells by Mesoporous Silica Nanoparticles

Amauri J. Paula,*[,‡,∥] Roberto T. Araujo Júnior,[§,∥] Diego Stéfani T. Martinez,[†] Edgar J. Paredes-Gamero,[§] Helena B. Nader,[§] Nelson Durán,[‡,#] Giselle Z. Justo,[§,⊥] and Oswaldo Luiz Alves*[,†]

[‡]Laboratório de Química Biológica and [†]Laboratório de Química do Estado Sólido, Instituto de Química, Universidade Estadual de Campinas, 13083-970, Campinas-SP, Brazil

[§]Departamento de Bioquímica, Universidade Federal de São Paulo (Campus São Paulo), 04044-020, São Paulo-SP, Brazil

[#]Centro de Ciências Naturais e Humanas, Universidade Federal do ABC, 09210-580, Santo André, SP, Brazil

[⊥]Departamento de Ciências Biológicas, Universidade Federal de São Paulo (Campus Diadema), 09972-270, Diadema-SP, Brazil

Supporting Information

ABSTRACT: Although there are several studies reporting the promising biological efficiency of mesoporous silica nanoparticles (loaded with antitumoral drugs) against cancer cells and tumors, there are no reports on the influence of the bio−nano interface interactions on the molecular diffusion process occurring along their pores. In this context, we show here that the protein coating formed on multifunctionalized colloidal mesoporous silica nanoparticles (MSNs) dispersed in a cell culture medium decreases the release of camptothecin (CPT, a hydrophobic antitumoral drug) from the pores of MSNs. This effect is related to the adsorption of biomolecules on the nanoparticle surface, which partially blocks the pores. Parallely, the hydrophobic functionalization inside the pores can offer suitable sites for the adsorption of other molecules present in the cell culture medium depending on the hydrophobicity, size, and conformation aspects of these molecules and adsorption sites of MSNs. Thus, the molecular cargo loaded in the pores (i.e. CPT) can be replaced by specific molecules present in the dispersion medium. As a consequence, we show that a non-permeable cellular staining molecule such as SYTOX green can be incorporated in MSNs through this mechanism and internalized by cells in an artificial fashion. By extrapolating this phenomenon for applications in vivo, one has to consider now the possible manifestation of unpredicted biological effects from the use of porous silica nanoparticles and others with similar structure due to these internalization aspects.

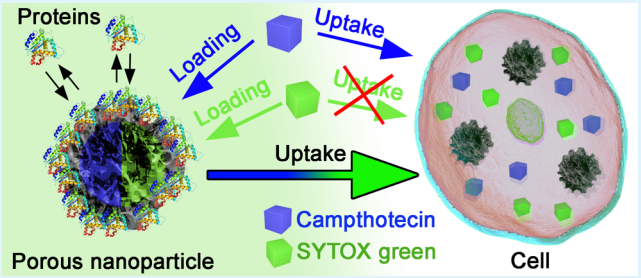

KEYWORDS: *mesoporous silica, colloidal nanoparticles, biomolecules' interaction, bovine serum albumin, protein corona, drug delivery*

1. INTRODUCTION

In the last decade there has been a growing number of creative approaches for the controlled release of molecules from mesoporous silica nanoparticles (MSNs) operating under the host−guest approach. Advances in this aspect are likely to impact a wide range of scientific and technological areas from industry to medicine. For instance, these nanostructures can be used as a tool to improve the theranosis of several diseases, including cancer.[1−9] In this context, the surface engineering of MSNs is a key point for the control of the molecular release from the pores of the nanostructure. A remarkable advance in this area was achieved through the design of efficient molecular stoppers on the pores of MSNs, which can be built with stimuli-responsive release mechanisms sensitive to pH,[10−12] enzymes,[13,14] photocleavable linkers,[15] temperature,[16,17] disulfide bond-reducing molecules,[18,19] and monosaccharides.[20] The main objective of these designs was to control the diffusion process of molecules from the internal pores to the external medium.

Certainly, important and fundamental knowledge has been accrued on the development of silica nanomaterials with various combinations of morphology, pore structure, and functionalization. However, when considering some nano-biotechnological applications, for instance, the intravenous administration of MSNs for medical therapies, more realistic approaches are required to develop efficient treatment options. For this reason the use of bio-friendly capping mechanisms and surface coatings on MSNs was initially proposed to overcome biocompatibility and toxicology issues.[5,6,13,17,21] Furthermore, another scientific approach has emerged and introduced new considerations regarding the supramolecular interactions occurring at the biofluid/nanomaterial interface. Studies revealed that the biological effects manifested from the use of nanomaterials are a result not only of the intrinsic character-

Received: April 21, 2013
Accepted: July 10, 2013
Published: July 10, 2013

   dx.doi.org/10.1021/am4014693 | ACS Appl. Mater. Interfaces 2013, 5, 8387−8393

istics of the nanomaterial and its surface, but rather of the characteristics of a new entity formed by the nanostructure and the biomolecules interacting with it in the biofluid.[22−32] These interactions occur at the bio−nano interface where a biomolecule coating (i.e. protein corona) or even a new hybrid complex may be formed depending on the biological environment in which the nanoparticle is inserted. From this perspective the cytotoxicity, for instance, will be affected by the biomolecular coating on the nanostructure, which varies as a function of the protein corona features[33] and the "cell vision"; the latter being related to the way that cells see this biomolecular−nanostructure entity.[34−36] Therefore, for several nanobiotechnological applications, it is now clear the necessity of using scientific models based on complexity, considering the integration, interaction, and multiplicity of the involved entities.

The delivery of molecules into cells and tissues by silica nanocarriers has been shown in several studies, which confirmed the in situ and in vivo efficiency of MSNs.[6,8,21,37−41] However, to the best of our knowledge, fundamental studies on the influence of the protein corona on the molecule diffusion process occurring along the pores of MSNs have not been reported. Possibly diffusion mechanisms in biofluids containing porous silica nanoparticles and other porous nanostructures will be altered as a function of these interactions at the bio−nano interface. By using spherical colloidal MSNs with a hydrophobic functionalization on the inner pores and a hydrophilic functionalization on the outer surface, and incorporated with camptothecin (CPT, a hydrophobic antitumoral drug), we show here that the protein corona on the surface of MSNs hampers but does not prevent the diffusion of CPT from the interior of the nanoparticle to the biofluid and that molecules in the biofluid have access to the internal hydrophobic environment of MSNs. Furthermore, as colloidal MSNs possess a broad internal functionalization with hydrophobic chemical groups (i.e. phenyl), specific molecules present in the dispersion medium (e.g. cell culture medium) can be loaded into the nanoparticles and internalized into living cells in an artificial fashion nonexistent in the absence of MSNs.

2. EXPERIMENTAL SECTION

2.1. Synthesis of Multifunctionalized Colloidal MSNs. MSNs with a size distribution range from 40 to 80 nm and large pore sizes were produced based on a sol−gel method as previously reported.[42] The methodology is a modification of the Stöber method,[43] which uses tetraethyl orthosilicate (TEOS) as the Si precursor, an alcohol (ethanol) as the homogenizing agent, and ammonia (NH_3) as the base catalyst. The synthesis is performed under high concentrations of precursors, thus resulting in monodisperse nanoparticles. To engineer the hydrophobic internal pores and the hydrophilic external surface of MSNs, a co-condensation process with organosilanes was used. For this, 750 mg of cetyltrimethylammonium bromide (CTAB) was dissolved in 20.0 mL of a NH_3 aqueous solution (0.05 mol L^{-1}, pH 11) and homogenized under magnetic stirring in a round-bottomed distillation flask attached to a reflux condenser at 5°C (to avoid ethanol evaporation). To this solution, 3.20 mL of absolute ethanol were added as the cosolvent, and the mixture was homogenized for 15 min at 60 °C. The internal porous structure was functionalized with phenyl radicals by using 1.49 mL of TEOS (6.72 mmol) and 816 μL of phenyltriethoxysilane (PTES, 3.36 mmol). This mixture was sonicated for 15 min prior to being transferred to the distillation flask. This first addition of silicon monomers (at t = 0 min) leads to the nucleation and growth of particles. After 60 minutes, time at which the majority of the silicon monomers were condensed as nanoparticles, another TEOS addition (124 μL, 0.56 mmol) was performed to create a non-functionalized SiO_2 shell to isolate the internal hydrophobic porous structure from the external surface during the decoration with hydrophilic groups. This was achieved over the period from 60−90 min. The last TEOS addition (at t = 90 min, 124 μL, 0.56 mmol) was done to form the outer shell of SiO_2. The hydrophilic functionalization of the outer surface was carried out during the formation of the outer shell by the addition of 128 μL of 3-(trihydroxysilyl)-propylmethylphosphonate (THSPMP) immediately after the last TEOS addition (at t = 90 min). The addition of THSPMP represented an increase in Si of 2.5%-mol (0.28 mmol) over the quantity previously added as TEOS and PTES (11.20 mmol). After the end of the reaction, products were isolated by centrifugation at 17 949 rcf and washed with absolute ethanol before extracting the soft-template (CTAB, see the Supporting Information for details). After the CTAB extraction, the colloidal porous nanoparticles were washed twice with absolute ethanol and resuspended in absolute ethanol and stored in the refrigerator. Aqueous suspensions of colloidal MSNs were produced by isolating the sample from the ethanolic suspension (by centrifugation), washing twice with deionized water, and resuspending it in deionized water. These suspensions were used for the biological assays.

2.2. CPT Incorporation and Evaluation of the Molecular Diffusion Process. The highly hydrophobic pores of the fabricated MSNs facilitate efficient loading of CPT. This molecule was incorporated in the pores of silica nanocarriers by sonicating the aqueous suspension of MSNs in the presence of CPT (added as a powder). The sonication process is necessary to break CPT particles and induce the molecule adsorption in the pores of nanoparticles. The determination of the loading capacity of MSNs was carried out by mixing the aqueous suspension of MSNs and CPT (as a powder) in an 10:1 MSNs:CPT weight-ratio. Nonincorporated CPT powders remained insoluble and were separated from the colloidal suspension by centrifugation at 500 rpm for 2 min. A volume of the colloidal suspension (w/CPT) was withdrawn and analysized through UV−vis absorption spectroscopy. To estimate the CPT amount in the MSNs, the spectrum for this mixture (red curve, see Figure S5 in the Supporting Information) was subtracted from the spectrum for MSNs without CPT (blue curve), thus resulting in the CPT spectrum with a zero-baseline. Subsequently, the area of the CPT absorption band at 350 nm was calculated and compared to a standard calibration curve (black curve and inset). It should be noted that, if the CPT powder is added in a quantity lower than the nanoparticle loading capacity (estimated at 3% w/w), the incorporation process is done in a single step without centrifugation.

The MSNs incorporated with CPT were incubated for 1 h at 37 °C in 1.0 mL of a cell culture medium (RPMI 1640 supplemented with 10% of fetal bovine serum, 100 U mL^{-1} of penicillin and 100 μg mL^{-1} of streptomycin) in order to generate the biomolecular coatings (protein corona). The final concentration of MSNs was 500 μg mL^{-1}. A duplicate incubation was also performed under the same conditions but in the absence of fetal bovine serum (FBS) in the medium. Nanoparticles were then centrifuged at 20 817 rcf for 30 min at 4°C and resuspended in 250 μL of a 0.1 μg mL^{-1} SYTOX green solution and incubated in the dark for 30 minutes at 37 °C. After this incubation period MSNs were again centrifuged and isolated from the supernatant. Quantification of the CPT release was done by measuring its fluorescence (excitation at 360 nm) in the isolated supernatant. Incorporation of SYTOX green into the MSNs was confirmed by resuspending the isolated nanoparticles and measuring their fluorescence at 480 nm (excitation). The same procedure was repeated for MSNs that were incubated in the culture medium in the absence of FBS. Analyses of mixtures of CPT and SYTOX green showed that spectra do not overlap.

2.3. Protein Corona Assays. To indentify biomolecules that strongly interact with colloidal MSNs, the "hard corona" was extracted from the surface of nanoparticles after their incubation period in RPMI 1640 containing FBS. For this, MSNs were used at the final concentration of 100 μg mL^{-1} (in 2.0 mL of culture medium). The incubation conditions were the same as previously described. Nanoparticles were then isolated by centrifugation (at 20 817 rcf for

1 h at 4 °C) and resuspended in a PBS solution (10.0 mmol L^{-1} of a phosphate buffer, 2.7 mmol L^{-1} of potassium chloride and 137 mmol L^{-1} of sodium chloride, pH 7.4). Three washing cycles with PBS solution were performed in order to remove weakly-bonded biomolecules (centrifugation at this step was performed at 20 817 rcf for 30 min at 4 °C). Finally, the pellet (MSNs containing strongly-bonded proteins) was resuspended in a protein loading buffer (150 μL, containing 62.5 mM of Tris-HCL, 2% (w/v) of SDS, 10% of glycerol, and 0.01% (w/v) of bromophenol blue; pH 6.8) and boiled for 3 min at 100 °C. From this resulting suspension, 15 μL was loaded in a 15% SDS-polyacrylamide gel. After running the electrophoresis, the gel was stained with coomassie blue in order to indentify hard corona proteins. Dynamic light scattering (DLS) and zeta potential (ζ) analyses of MSNs with the hard corona were carried out after the PBS washing procedure. For this, instead of being resuspended in the protein loading buffer, the pellet was resuspended in deionized water. All assays described here were performed in triplicate.

2.4. Confocal Microscopy Study. Colorectal cancer cells (HCT 116) were grown in 24-well microplates (1×10^4 cells per well) on glass coverslips for 24 h in RPMI 1640 supplemented with 10% of FBS, 100 U mL^{-1} of penicillin and 100 μg mL^{-1} of streptomycin. Cells were maintained in a humidified incubator containing 5% CO_2 at 37 °C, and incubated for 4 h in the same conditions with CPT-loaded colloidal MSNs (100 μg mL^{-1} containing 3 μg mL^{-1} of CPT) or CPT solubilized in dimethyl sulfoxide (3 μg mL^{-1}; with a final solvent concentration lower than 0.1% [v/v] to prevent cell damage). Cells were then washed with a Hank's Balanced Salt Solution (HBSS) and incubated with WGA-Alexa Fluor 594 (3 μg mL^{-1}, a cell membrane stain) for 30 min and washed twice. Afterwards, they were fixed with 2% of paraformaldehyde for 30 min, washed with HBSS containing 0.1 mol L^{-1} of glycine, and then permeabilized in HBSS containing 0.01% of saponin for 20 min. Finally, cells were incubated with the DNA stain SYTOX green (0.1 μg mL^{-1}) and the CPT uptake was evaluated by confocal microscopy. The same procedure was performed for CPT-loaded MSNs without the permeation step for staining the nucleus. SYTOX green was excited with an argon laser (λ_{Ex} = 488 nm, λ_{Em} = 500−550 nm), WGA-Alexa Fluor 594 was excited with a HeNe laser (λ_{Ex} = 594 nm, λ_{Em} = 600−640 nm) and CPT was excited with a two-photon laser (λ_{Ex} = 740 nm, λ_{Em} = 430−490 nm).

3. RESULTS AND DISCUSSION

The antagonistic hydrophobic and hydrophilic functionalizations of the colloidal MSNs with phenyl (inner pores) and methylphosphonate (outer surface) groups, respectively, were confirmed through ^{29}Si and ^{13}C nuclear magnetic resonance (NMR) in the high-power decoupling (HPDEC) mode and cross-polarization and magic angle spinning mode (CPMAS, see Figures S1 and S2 in the Supporting Information). The identification in spectra was done for silicon sites associated with Si−phenyl bonds as well as for each carbon atom related to the functionalizing organic groups. A high density of phenyl groups was co-condensed on the inner pores of silica nanoparticles: ∼23%-mol of Si, nearly a half of all surface sites (considering P^2, P^3, Q^2, and Q^3). The nanoparticle size distribution ranged from 40 to 80 nm, as determined by transmission electron microscopy (TEM) images by measuring the Feret's diameter of more than 100 nanoparticles (see Figure S3 in the Supporting Information). The porous structure of the hydrophobic silica nanocarrier was determined by N_2 adsorption−desorption isotherms and pore size distribution curves (see Figure S4 in the Supporting Information), and also through scanning transmission electron microscopy (STEM), shown in Figure 1. The STEM image indicates the presence of pores larger than 5 nm, in agreement with the pore size distribution. According to dynamic light scattering (DLS) and zeta potential measurements, the nanoparticles are monodisperse (low PDI value), possess an average size of 120 nm,

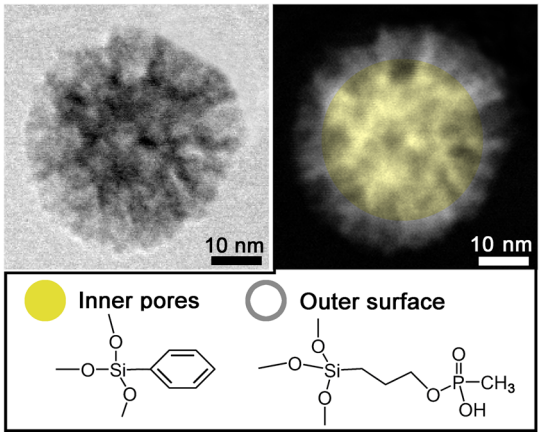

Figure 1. Scanning transmission electron microscopy images in the bright-field mode (BF-STEM, left panel) and in the high-annular dark-field mode (HAADF-STEM, right panel). A diagram representing the hierarchical organic functionalizations of the hydrophobic silica nanocarrier is also shown.

and contain a negatively charged surface as a result of the deprotonation of propylmethylphosphonate and silanol groups (see Table 1).

Until 2006, about 40% of small-molecule drugs developed by pharmaceutical companies had limited or no application due to their low aqueous solubility, which hampers their administration.[44] Camptothecin, an inhibitor of the DNA topoisomerase I enzyme is included in this percentage. In this research, this problem was addressed by delivering CPT into cells through colloidal MSNs containing hydrophobic pores and a hydrophilic surface modification, allowing transportation in aqueous and biological media. As a result of the nanocarrier characteristics, namely, a broad hydrophobic internal coverage and a long-term colloidal stability, CPT can be easily incorporated into the pores of nanoparticles by simply mixing an aqueous colloidal suspension of MSNs with CPT powders. The sonication of this mixture is enough to overcome all energetic barriers involved in the particle breaking and in the molecule absorption on silica nanoparticles. The loading capacity of MSNs through this method was of 3% (w/w) for CPT. Propylmethylphosphonate groups externally condensed on the surface of colloidal MSNs provide long term stability for the nanocarrier when compared to nanoparticles containing just silanol groups on the external surface (see Figure S6 in the Supporting Information). After the incubation for 1 h in an RPMI cell culture medium containing FBS, a biomolecular coating developed on the surface of the silica nanoparticle. This phenomenon was confirmed through dynamic light scattering (DLS) analyses of nanoparticles after their incubation and isolation. The increase in the hydrodynamic radius is a result of the presence of strongly-bonded biomolecules on MSNs, referred to as a "hard corona". The zeta potential value did not vary indicating that the electrokinetic potential of the colloidal suspension remained the same after corona formation (see Table 1).

As CPT is largely insoluble in water, a measured quantity of this molecule is promptly released with the dispersion of CPT-loaded MSNs in water and this amount does not vary over time, since it is limited by the low solubility of CPT. However, as a result of the formation of the biomolecular coating the CPT diffusion process from the pores to the medium is altered. After the MSNs were incubated in the cell culture medium and

Table 1. Physicochemical Characteristics of Multifunctionalized Colloidal MSNs

			DLS analysis[c]		zeta potential (ζ)[e]	
sample	surface area[a] ($m^2\ g^{-1}$)	pore volume[b] ($cm^3\ g^{-1}$)	average size (nm)	PDI[d]	value (mV)	STD (mV)[f]
s-nanocarrier	950	2.1	120 ± 18	0.162 ± 0.04	−30.5	6.8
HC s-nanocarrier[g]			234 ± 21	0.232 ± 0.01	−29.5	6.8

[a]Calculated from the N_2-adsorption branch by using the BET method. [b]Evaluated through the single-point value adsorbed at P/P_0 = ~0.94. [c]Analyses performed in deionized water. [d]Polydispersity index. [e]Measured with a suspension of nanoparticles in a 1 mmol L^{-1} KCl solution. [f]STD = standard deviation. [g]HC stands for hard corona.

isolated, the CPT release was evaluated by measuring the fluorescence spectrum of the resulting supernatant after the centrifugation of the colloidal suspension (see Figure 2a). With the formation of the protein corona, less CPT was released compared to the amount of CPT released from uncoated nanoparticles (i.e., MSNs incubated in the cell culture medium without FBS). The difference observed in Figure 2a could be detected because the protein corona hampers the diffusion process in a way that the amount released (blue curve in Figure 2a) is below the CPT solubility (black curve in Figure 2a). The use of phospholipid bilayers fused on porous silica nanoparticle as coatings has proven to be an efficient approach to prevent the displacement of hydrophilic molecules from the pores, mainly due to the adsorption of polyvalent ions such as phosphate, sulfate, and carbonate.[45] However, when dispersed in complex biological fluids, such as the cell culture medium used here, proteins (and other biomolecules) adsorbed on bare porous nanoparticles can interfere with this molecular displacement similarly to phospholipid bilayers fused on MSNs.

The identification of proteins present in the hard corona (strongly-bonded proteins) can provide useful information regarding the existence of selective interactions between the nanoparticle and biomolecules of the biofluid. Sodium dodecyl sulfate polyacrylamide gel electrophoresis (SDS-PAGE), represented in Figure 2b, shows a broad distribution of proteins that interacted with MSNs. Specific bands indicate a major presence of proteins around 10, 25, 50, and above 100 kDa. There are several studies in the literature associating the distribution of hard corona proteins as a function of the concentration of biomolecules and nanoparticle composition, size, and surface functionalizations.[29,32] However, considering the porous structure of silica nanocarriers, which results in an irregular surface topography, a biomolecular adsorption mechanism based on size-matching considerations must also be considered. For instance, as it the most available protein in FBS, with dimensions of 7.5 × 6.5 × 4.0 nm and a molecular weight around 66 kDa, bovine serum albumin (BSA) could be inserted in the pores of nanocarriers through a size matching regardless of the surface charge of both entities.[46] Smaller biomolecules can face the same fate. Furthermore, after the insertion of biomolecules into a nanoparticle pore others can adsorb on the first layers coating the surface, thus reducing the surface free energy.

In order to evaluate the behavior of silica nanocarriers (w/ CPT) in the presence of HCT 116 cells, confocal microscopy analyses were carried out by using staining molecules for the nucleus (SYTOX green, which binds to DNA) and cell membrane (WGA Alexa Fluor 594, a wheat germ agglutinin conjugated with a fluorophore that binds to *N*-acetylglucosamine and *N*-acetylneuraminic acid residues present in cell surface glycoproteins on the plasma membrane). Cells were treated with CPT at a concentration of 3 μg mL^{-1} (8.6 nmol mL^{-1}), and its internalization into cells was confirmed by the blue fluorescence-emission (see Figure 3a). When CPT was added at the same concentration but loaded in silica nanocarriers (100 μg mL^{-1}), this molecule was observed inside

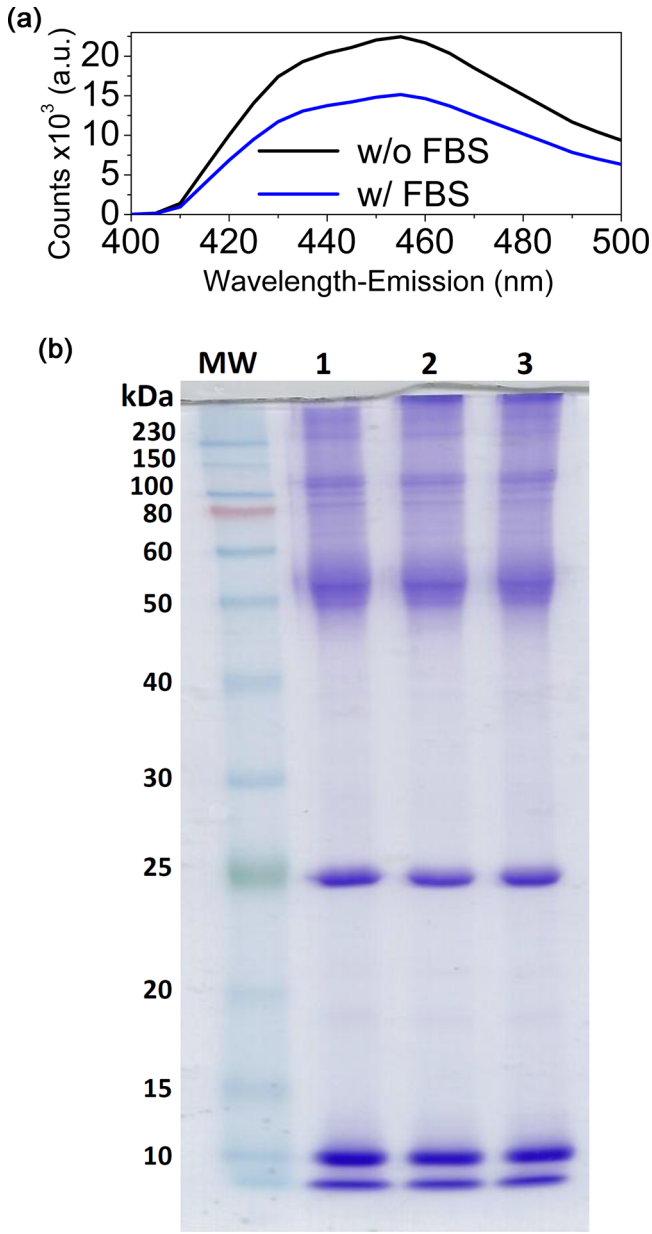

Figure 2. (a) Fluorescence spectra of CPT released from silica nanocarriers in a RPMI 1640 culture medium in the presence (w/ FBS) or absence (w/o FBS) of fetal bovine serum proteins. (b) SDS-PAGE of the hard corona proteins extracted from silica nanoparticles after the incubation in the cell culture medium containing FBS. The MW lane contains molecular weight protein standards; lanes 1−3 are independent triplicates.

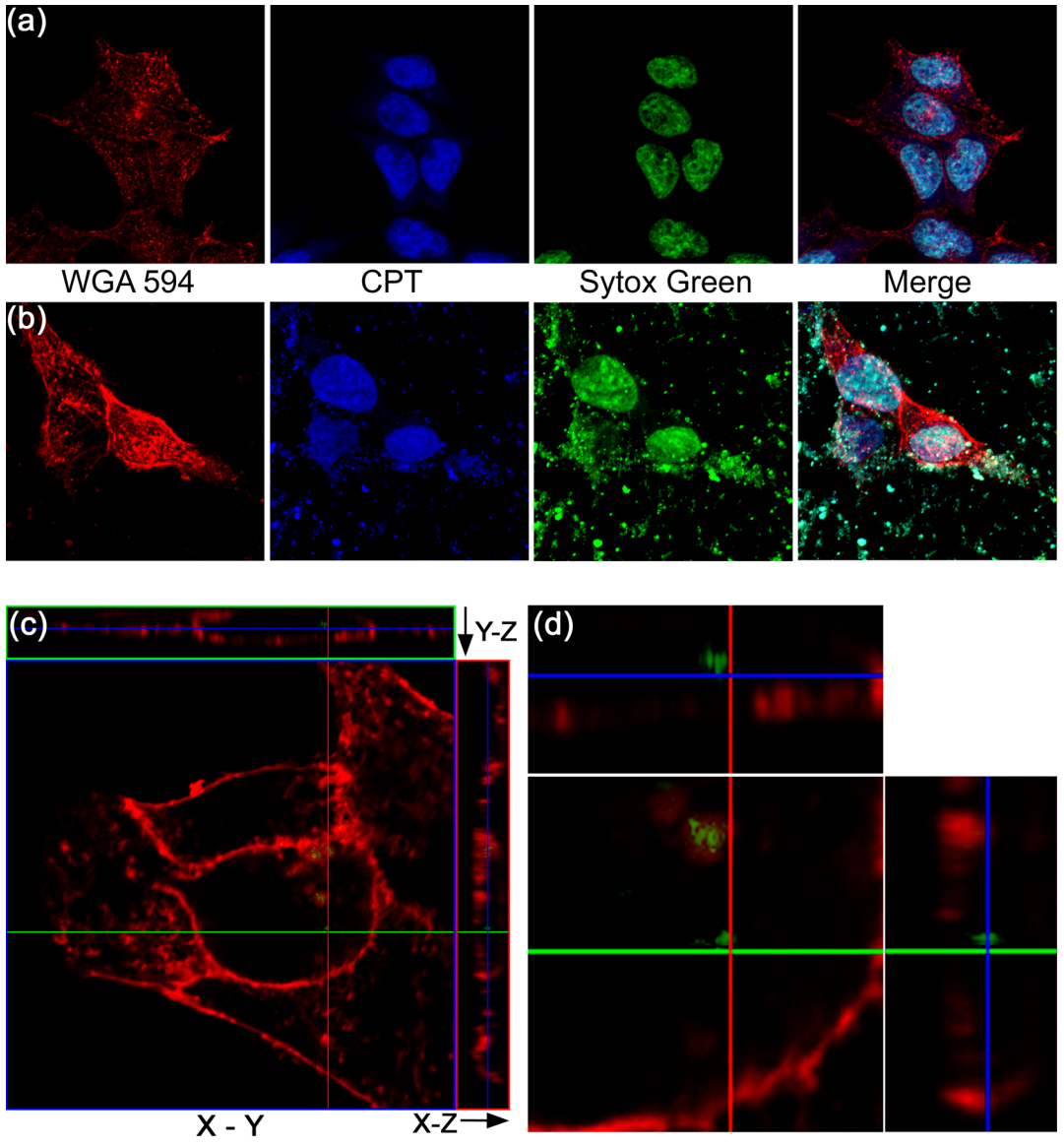

Figure 3. Confocal microscopy images of HCT 116 cells incubated with (a) camptothecin and (b) hydrophobic silica nanocarriers with camptothecin. Images were taken with emission wavelengths in red (for cell membranes stained with WGA 594), blue (for CPT), and green (cell nuclei stained with SYTOX green). The image with the merged colors is also presented. (c) Image showing the incorporation of SYTOX green into cells by hydrophobic silica nanocarriers. (d) Enlargement of the image presented in part c.

and outside the nucleus, as well as outside the cells. The CPT fluorescence overlaps that of SYTOX green (green), thus indicating the fluorophore incorporation in silica nanocarriers (see Figure 3b). Light emission outside the cells for both CPT and SYTOX green is a result of the attachment of silica nanoparticles on the glass slide, upon which they strongly adsorb and are not removed by the washing process. The cellular uptake of silica nanocarriers and their ability to transport SYTOX green into cells were confirmed through the green fluorescence in the $x-z$ and $y-z$ image planes (see Figures 3c and d). These images were taken in the absence of the cell permeation procedure, which must otherwise be performed in order to allow the SYTOX green internalization and to induce nuclear staining, since this fluorophore is a membrane−impermeable DNA binder. The incorporation observed for SYTOX green (see Figure S7 in the Supporting Information) was also confirmed for the fluorophore 7AAD (7-aminoactinomycin D, a molecular stain for DNA). In contrast, wheat germ agglutinin (WGA 594), with a molecular weight of approximately 38 kDa did not interact with the MSNs to the extent that the smaller fluorescent molecules did (SYTOX green and 7AAD). In addition, the fluorophore Lucifer yellow was not incorporated into the porous silica nanoparticles. Therefore, the internalization of extracellular molecules into cells by silica nanocarriers will depend on charge, hydrophobicity, size, and molecular conformation aspects, which will determine the interaction between these entities (see the fluorophores molecular structures in Figure S8 in the Supporting Information) and the adsorption sites in the nanocarrier pores. For instance, the hydrophobic microchemical environment present in the inner pores of the colloidal MSNs used here can favor specific supramolecular interactions with poly-aromatic molecules through van der Waals forces and pi-stacking bonds.[47]

Therefore, molecular diffusion phenomena in biological fluids containing silica nanocarriers will be ruled by complex

dx.doi.org/10.1021/am4014693 | ACS Appl. Mater. Interfaces 2013, 5, 8387−8393

kinetic and thermodynamic aspects that are directly related to the surface microchemical environment of the nanostructure and the protein corona features (Figure 4a). By considering a

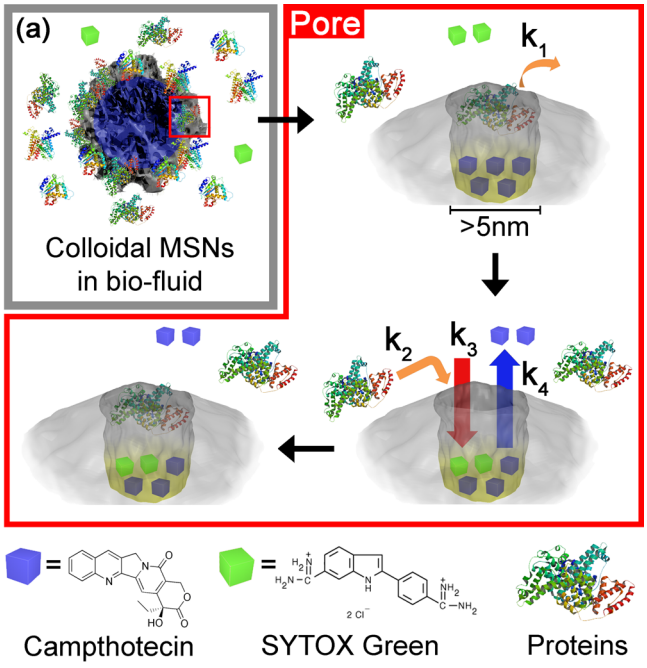

Figure 4. (a) Scheme illustrating pore obstruction due to the adsorption of biomolecules and the molecular diffusion process (for CPT and SYTOX green) occurring in silica nanocarriers with a hydrophobic microchemical environment in the pores. (b) Representation of the cellular uptake process for hydrophobic silica nanocarrier incorporated with camptothecin and SYTOX green.

situation of pore blocking by the proteins, the incorporation (k_3) and release (k_4) mechanisms for two different molecules possessing affinity to the internal microchemical environment of the nanocarrier (e.g. CPT and SYTOX green) will occur not only as a function of their adsorption−desorption kinetic constants but also of the protein adsorption−desorption constants (k_1 and k_2). In other conditions, such as with nanoparticles with large pore sizes, the molecular diffusion processes can occur with less dependence on the protein corona. On the other hand, smaller pore holes might increase the integration level between these constants. Therefore, access to the internal cavities of porous nanocarriers may lead to the incorporation of extracellular molecules which have affinity with the pore microchemical environment, thus resulting in their insertion into cells (Figure 4b). To prevent this event, a programmable molecular stopper operating in this context will face the difficult requirement of hindering the access of molecules to the inner cavities of the nanoparticle until it is inserted in the target living entity.

4. CONCLUSIONS

In summary, we reported here that the chemical interactions occurring at the bio−nano interface of colloidal MSNs (with a hydrophobic internal environment) in a cell culture medium (i.e. RPMI 1640 containing 10% of FBS) influences the diffusion mechanism through which molecules (e.g. CPT) will be released from the internal pores to the external medium. In addition, molecules present in the cell culture medium (e.g. SYTOX green) can also replace drugs (e.g. CPT) in the hydrophobic pore cavities of the silica nanocarrier as a result of the chemical affinity between these entities. As the nanocarrier can be internalized by cells, it may transport these extracellular molecules (e.g. SYTOX green) adsorbed on the inner pores, thus resulting in an artificially-induced internalization event. These findings must be considered in all perspectives involving the use of MSNs and other nanostructures (containing internal cavities) as molecular vehicles to reach cells and tissues since this phenomenon may result in unexpected and undesired biological effects. Although the nanocarrier efficiency in delivering the molecular cargo into specific cells and tissues will be ruled by complex kinetic and thermodynamic mechanisms (in a nonsteady state), an optimization of the nanocarrier efficiency can be achieved with our current synthetic tools. By changing the pore size, a variation in molecular diffusion process will be induced through size-matching aspects between the pore cavity (s_p) and biomolecules from the protein corona (s_b). With small pores, a wide variety of proteins from the biofluid can block the pore holes ($s_b > s_p$), thus inhibiting the release of small molecules and restricting the access of molecules from the medium to the nanoparticle internal cavity.

■ ASSOCIATED CONTENT

Supporting Information

More details regarding reagents and synthetic protocols; biological assays; nuclear magnetic resonance (NMR), fluorescence, and UV−vis light absorption spectra; thermogravimetric and N_2-sorption isotherm analyses; and transmission electron microscopy (TEM) images. This material is available free of charge via the Internet at http://pubs.acs.org.

■ AUTHOR INFORMATION

Corresponding Author

*E-mail: amaurijp@gmail.com; oalves@iqm.unicamp.br.

Author Contributions

‖A.J.P. and R.T.A.J.: These authors contributed equally for the elaboration of this paper.

Notes

The authors declare no competing financial interest.

■ ACKNOWLEDGMENTS

The authors thank FAPESP; CAPES; CNPq; and INCT-Inomat and the Brazilian Nanotoxicology (CIGeNanotox-CNPq) Network Programs for financial support. The authors also thank Dr. Matthew J. Grossman for general discussion and revision of this work.

■ REFERENCES

(1) Ashley, C. E.; Carnes, E. C.; Phillips, G. K.; Padilla, D.; Durfee, P. N.; Brown, P. A.; Hanna, T. N.; Liu, J. W.; Phillips, B.; Carter, M. B.; Carroll, N. J.; Jiang, X. M.; Dunphy, D. R.; Willman, C. L.; Petsev, D. N.; Evans, D. G.; Parikh, A. N.; Chackerian, B.; Wharton, W.; Peabody, D. S.; Brinker, C. J. *Nat. Mater.* **2011**, *10*, 389−397.
(2) Idris, N. M.; Gnanasammandhan, M. K.; Zhang, J.; Ho, P. C.; Mahendran, R.; Zhang, Y. *Nat. Med.* **2012**, *18*, 1580−1586.
(3) Vallet-Regi, M.; Ramila, A.; del Real, R. P.; Perez-Pariente, J. *Chem. Mater.* **2001**, *13*, 308−311.
(4) Lu, J.; Liong, M.; Zink, J. I.; Tamanoi, F. *Small* **2007**, *3*, 1341−1346.
(5) Argyo, C.; Cauda, V.; Engelke, H.; Radler, J.; Bein, G.; Bein, T. *Chem.—Eur. J.* **2012**, *18*, 428−432.
(6) Li, X.; Chen, Y. J.; Wang, M. Q.; Ma, Y. J.; Xia, W. L.; Gu, H. C. *Biomaterials* **2013**, *34*, 1391−1401.
(7) Knezevic, N. Z.; Trewyn, B. G.; Lin, V. S. Y. *Chem.—Eur. J.* **2011**, *17*, 3338−3342.
(8) Wu, S. H.; Hung, Y.; Mou, C. Y. *Chem. Commun.* **2011**, *47*, 9972−9985.
(9) Wang, T. T.; Zhang, L. Y.; Su, Z. M.; Wang, C. G.; Liao, Y.; Fu, Q. *ACS Appl. Mater. Interfaces* **2011**, *3*, 2479−2486.
(10) Angelos, S.; Khashab, N. M.; Yang, Y. W.; Trabolsi, A.; Khatib, H. A.; Stoddart, J. F.; Zink, J. I. *J. Am. Chem. Soc.* **2009**, *131*, 12912−12914.
(11) Zhao, Y. L.; Li, Z. X.; Kabehie, S.; Botros, Y. Y.; Stoddart, J. F.; Zink, J. I. *J. Am. Chem. Soc.* **2010**, *132*, 13016−13025.
(12) Chang, B. S.; Guo, J.; Liu, C. Y.; Qian, J.; Yang, W. L. *J. Mater. Chem.* **2010**, *20*, 9941−9947.
(13) Schlossbauer, A.; Kecht, J.; Bein, T. *Angew. Chem. Int. Ed.* **2009**, *48*, 3092−3095.
(14) Patel, K.; Angelos, S.; Dichtel, W. R.; Coskun, A.; Yang, Y. W.; Zink, J. I.; Stoddart, J. F. *J. Am. Chem. Soc.* **2008**, *130*, 2382−2383.
(15) Vivero-Escoto, J. L.; Slowing, I. I.; Wu, C. W.; Lin, V. S. Y. *J. Am. Chem. Soc.* **2009**, *131*, 3462−3463.
(16) You, Y. Z.; Kalebaila, K. K.; Brock, S. L.; Oupicky, D. *Chem. Mater.* **2008**, *20*, 3354−3359.
(17) Schlossbauer, A.; Warncke, S.; Gramlich, P. M. E.; Kecht, J.; Manetto, A.; Carell, T.; Bein, T. *Angew. Chem. Int. Ed.* **2010**, *49*, 4734−4737.
(18) Lai, C. Y.; Trewyn, B. G.; Jeftinija, D. M.; Jeftinija, K.; Xu, S.; Jeftinija, S.; Lin, V. S. Y. *J. Am. Chem. Soc.* **2003**, *125*, 4451−4459.
(19) Ferris, D. P.; Lu, J.; Gothard, C.; Yanes, R.; Thomas, C. R.; Olsen, J. C.; Stoddart, J. F.; Tamanoi, F.; Zink, J. I. *Small* **2011**, *7*, 1816−1826.
(20) Zhao, Y. N.; Trewyn, B. G.; Slowing, I. I.; Lin, V. S. Y. *J. Am. Chem. Soc.* **2009**, *131*, 8398−8400.
(21) Ashley, C. E.; Carnes, E. C.; Epler, K. E.; Padilla, D. P.; Phillips, G. K.; Castillo, R. E.; Wilkinson, D. C.; Wilkinson, B. S.; Burgard, C. A.; Kalinich, R. M.; Townson, J. L.; Chackerian, B.; Willman, C. L.; Peabody, D. S.; Wharton, W.; Brinker, C. J. *ACS Nano* **2012**, *6*, 2174−2188.
(22) Lesniak, A.; Campbell, A.; Monopoli, M. P.; Lynch, I.; Salvati, A.; Dawson, K. A. *Biomaterials* **2010**, *31*, 9511−9518.
(23) Deng, Z. J.; Mortimer, G.; Schiller, T.; Musumeci, A.; Martin, D.; Minchin, R. F. *Nanotechnology* **2009**, *20*, 455101−9.
(24) Lynch, I.; Salvati, A.; Dawson, K. A. *Nat. Nanotechnol.* **2009**, *4*, 546−547.
(25) Lundqvist, M.; Stigler, J.; Elia, G.; Lynch, I.; Cedervall, T.; Dawson, K. A. *Proc. Natl. Acad. Sci. USA* **2008**, *105*, 14265−14270.
(26) Walczyk, D.; Bombelli, F. B.; Monopoli, M. P.; Lynch, I.; Dawson, K. A. *J. Am. Chem. Soc.* **2010**, *132*, 5761−5768.
(27) Monopoli, M. P.; Walczyk, D.; Campbell, A.; Elia, G.; Lynch, I.; Bombelli, F. B.; Dawson, K. A. *J. Am. Chem. Soc.* **2011**, *133*, 2525−2534.
(28) Tenzer, S.; Docter, D.; Rosfa, S.; Wlodarski, A.; Kuharev, J.; Rekik, A.; Knauer, S. K.; Bantz, C.; Nawroth, T.; Bier, C.; Sirirattanapan, J.; Mann, W.; Treuel, L.; Zellner, R.; Maskos, M.; Schild, H.; Stauber, R. H. *ACS Nano* **2011**, *5*, 7155−7167.
(29) Monopoli, M. P.; Aberg, C.; Salvati, A.; Dawson, K. A. *Nat. Nanotechnol.* **2012**, *7*, 779−786.
(30) Mahmoudi, M.; Lynch, I.; Ejtehadi, M. R.; Monopoli, M. P.; Bombelli, F. B.; Laurent, S. *Chem. Rev.* **2011**, *111*, 5610−5637.
(31) Jedlovszky-Hajdu, A.; Bombelli, F. B.; Monopoli, M. P.; Tombacz, E.; Dawson, K. A. *Langmuir* **2012**, *28*, 14983−14991.
(32) Nel, A. E.; Madler, L.; Velegol, D.; Xia, T.; Hoek, E. M. V.; Somasundaran, P.; Klaessig, F.; Castranova, V.; Thompson, M. *Nat. Mater.* **2009**, *8*, 543−557.
(33) Paula, A. J.; Martinez, D. S. T.; Araujo, R. T.; Souza, A. G.; Alves, O. L. *J. Brazil. Chem. Soc.* **2012**, *23*, 1807−1814.
(34) Shapero, K.; Fenaroli, F.; Lynch, I.; Cottell, D. C.; Salvati, A.; Dawson, K. A. *Mol. Biosyst.* **2011**, *7*, 371−378.
(35) Mahmoudi, M.; Saeedi-Eslami, S. N.; Shokrgozar, M. A.; Azadmanesh, K.; Hassanlou, M.; Kalhor, H. R.; Burtea, C.; Rothen-Rutishauser, B.; Laurent, S.; Sheibani, S.; Vali, H. *Nanoscale* **2012**, *4*, 5461−5468.
(36) Laurent, S.; Burtea, C.; Thirifays, C.; Rezaee, F.; Mahmoudi, M. *J. Colloid Interface Sci.* **2013**, *392*, 431−445.
(37) Slowing, I. I.; Vivero-Escoto, J. L.; Trewyn, B. G.; Lin, V. S. Y. *J. Mater. Chem.* **2010**, *20*, 7924−7937.
(38) Veeranarayanan, S.; Poulose, A. C.; Mohamed, M. S.; Varghese, S. H.; Nagaoka, Y.; Yoshida, Y.; Maekawa, T.; Kumar, D. S. *Small* **2012**, *8*, 3476−3489.
(39) Lu, J.; Li, Z. X.; Zink, J. I.; Tamanoi, F. *Nanomed. Nanotechnol. Biol. Med.* **2012**, *8*, 212−220.
(40) Lee, J. E.; Lee, N.; Kim, T.; Kim, J.; Hyeon, T. *Acc. Chem. Res.* **2011**, *44*, 893−902.
(41) Rosenholm, J. M.; Sahlgren, C.; Linden, M. *Nanoscale* **2010**, *2*, 1870−1883.
(42) Paula, A. J.; Montoro, L. A.; Souza Filho, A. G.; Alves, O. L. *Chem. Commun.* **2012**, *48*, 591−593.
(43) Stober, W.; Fink, A.; Bohn, E. *J. Colloid Interface Sci.* **1968**, *26*, 62−69.
(44) Wagner, V.; Dullaart, A.; Bock, A. K.; Zweck, A. *Nat. Biotechnol.* **2006**, *24*, 1211−1217.
(45) Liu, J. W.; Jiang, X. M.; Ashley, C.; Brinker, C. J. *J. Am. Chem. Soc.* **2009**, *131*, 7567−7569.
(46) Puddu, V.; Perry, C. C. *ACS Nano* **2012**, *6*, 6356−6363.
(47) Grimme, S. *Angew. Chem. Int. Ed.* **2008**, *47*, 3430−3434.